Laminated Fe-34.5 Mn-0.04C composite with high strength and ductility

Wang, Yuhui; Kang, Jianmei; Peng, Yan; Wang, Tiansheng; Hansen, Niels; Huang, Xiaoxu

Published in:
Journal of Materials Science & Technology

Link to article, DOI:
10.1016/j.jmst.2018.05.013

Publication date:
2018

Document Version
Peer reviewed version

Laminated Fe-34.5Mn-0.04C composite with high strength and ductility

Yuhui Wang[1,2], Jianmei Kang[1], Yan Peng[2], Tiansheng Wang[1*], Niels Hansen[3] and Xiaoxu Huang[4,5*]

[1]*State Key Laboratory of Metastable Materials Science and Technology, Yanshan University, Qinhuangdao 066004, China*

[2]*National Engineering Research Center for Equipment and Technology of Cold Strip Rolling, Yanshan University, Qinhuangdao 066004, China*

[3]*Risø Campus, Technical University of Denmark, DK-4000 Roskilde, Denmark*

[4]*College of Materials Science and Engineering, Chongqing University, Chongqing 400045, China*

[5]*Department of Mechanical Engineering, Technical University of Denmark, DK-2800 Lyngby, Denmark*

[Received 03 February 2018; Received in revised form 03 March 2018; Accepted x xxxx 2018]

* *Corresponding author email:* tswang@ysu.edu.cn; xihu@mek.dtu.dk

To obtain a good combination of strength and ductility, a laminated composite structure composed of recovered hard lamellae and soft recrystallized lamellae has been produced in a single phase austenitic Fe-34.5Mn-0.04C steel by cold rolling and partial recrystallization. Enhanced mechanical properties in both strength and ductility have been obtained in the composite structure compared to a fully recrystallized coarse grain structure. A further increase in strength with only minor loss in total elongation has been achieved by a slight cold rolling of the composite structure, which also removes the small yield drop and Lüders elongation observed in the composite structure.

Keywords: Laminated composite structure; partial recrystallization; constraint effect, strength; ductility.

1. Introduction

An optimization of strength and ductility of metals and alloys for engineering application is of high current interest [1-6]. To obtain high strength by structural refinement for example by plastic deformation is well explored, but typically an increase in strength is followed by a severe drop in ductility [1-3,7,8]. An optimization has been sought through the design of microstructures containing hard and soft regions contributing to strength and ductility, respectively. Examples are a bimodal distribution of grain sizes in Cu [9] and a heterogeneous lamella structure in Ti [10]. In both cases, the processing route is rolling and annealing and the structure is subdivided by low, medium and high angle boundaries. The medium and high angle boundaries are geometrically necessary boundaries (GNBs) [11, 12] which delineate regions that deform with different slip systems or with different strain partitioning on the same systems [11, 13]. These boundaries can act as barriers to dislocation glide and their strength contribution increases as their distance decreases [14]. This distance increases when the deformed structure coarsens during recovery and recrystallization [15]. When the coarsening is heterogeneous the recovered or partially recrystallized structure is subdivided into bands: recovered regions and recrystallized regions [16,17]. Such a banded structure is a laminated composite structure of single phase composed of hard (recovered) and soft (recrystallized) layers, contributing respectively to strength and ductility.

In the present study, a laminated composite structure of hard recovered layers and soft recrystallized layers in a single high manganese phase austenitic steel is produced by cold rolling and partial recrystallization. High manganese austenitic steels show high tensile strength, high work hardening rate and superior plasticity at ambient and low temperatures due to the transformation-induced plasticity (TRIP) twinning-induced plasticity (TWIP) effects [18-22]. Therefore, they have potential applications as vehicle body material and cryogenic alloys for example used for liquefied natural gas tankage. However, they often have a disadvantage of a relatively low yield strength. Therefore, an objective of the present study is to enhance the yield strength of the high manganese

austenitic steel by microstructural design. The microstructural parameters and the tensile properties are determined and three characteristic samples are chosen for analysis. These samples are in the cold deformed, partially recrystallized and recrystallized state. It is demonstrated that an excellent combination of high yield strength and tensile ductility can be obtained from the sample with the laminated composite structure.

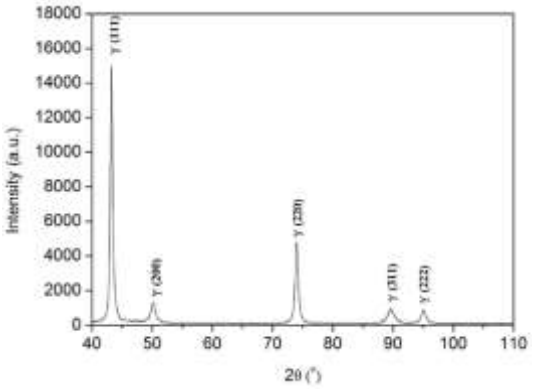

Fig. 1. X-ray diffractograms of sample after 90% CR

2. Material and processing

An austenitic steel with a nominal composition of Fe-34.5Mn-0.04C was used in this study. This steel is characterized by a higher manganese content than typical TWIP steels [19-22], and it does not show TWIP effect due to a relatively high stacking fault energy, but may have even higher toughness than typical TWIP steels [18]. An ingot was produced using a vacuum induction furnace, and then forged in the temperature range of 800 - 1100°C to form a 13 mm thick plate, in order to obtain a suitable thickness for cold rolling. The plate was then cold rolled to a thickness reduction of 90% using a laboratory rolling mill with a roll diameter of 230 mm. The cold rolled steel was annealed for 1 hour at 600°C and 1000°C to produce partially recrystallized and fully recrystallized structures, respectively. Due to the content of high manganese, the steel had a stable austenitic structure down to liquid nitrogen temperature. No martensitic transformation occurred during cold rolling, which was confirmed by X-ray

diffraction (XRD) using Rigaku D/Max 2500 diffractometer (see Fig.1). Therefore, in the present study, all the samples have a single phase austenitic structure.

The samples in the cold rolled, partially recrystallized and fully recrystallized states were subjected to microstructural characterization and tensile testing. The microstructure was characterized by transmission electron microscopy (TEM) with a JEM-2100 electron microscope operated at 200 kV, and by scanning electron microscopy (SEM) and electron backscatter diffraction (EBSD) with a Hitachi S-3400N-II scanning electron microscope. The step size for the EBSD scanning was 100 nm. All the microstructural observations were conducted on the longitudinal section containing the rolling direction (RD) and the normal direction (ND).

Tensile specimens with 10 mm in gage length and 5 mm in gage width were prepared such that the tensile direction was parallel to the RD. Tensile tests were carried out using a Zwick Z050TEW tensile machine at ambient temperature with an initial strain rate of $10^{-3}s^{-1}$. An extensometer was attached on the specimen during the tensile test for a precise measurement of tensile strain.

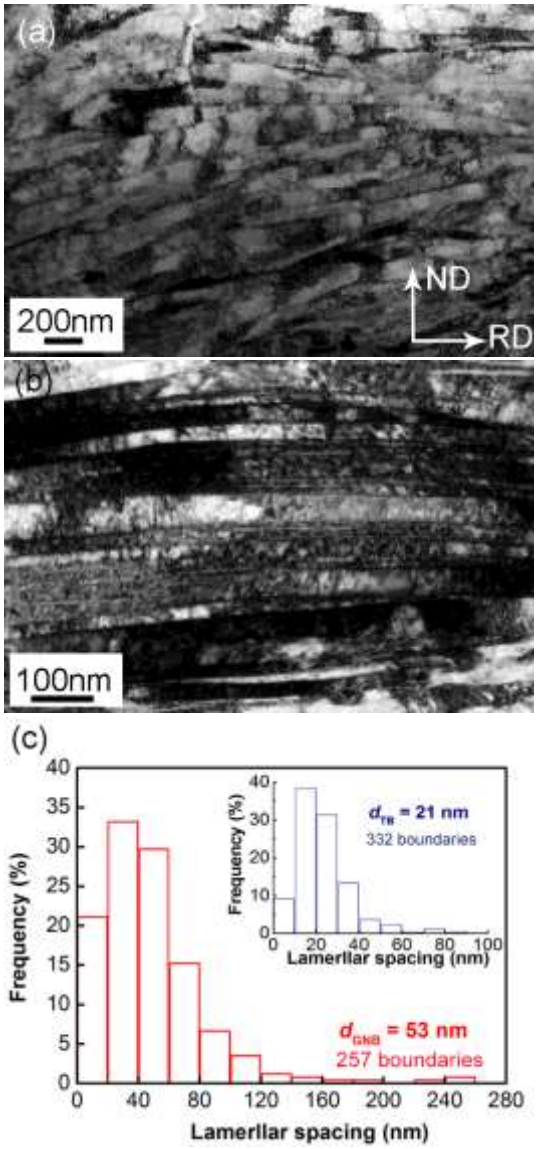

Fig. 2. TEM images of lamellar structures delineated by (a) GNBs and (b) TBs, and (c) the distribution of boundary spacings for GNBs and TBs in the 90% cold rolled sample.

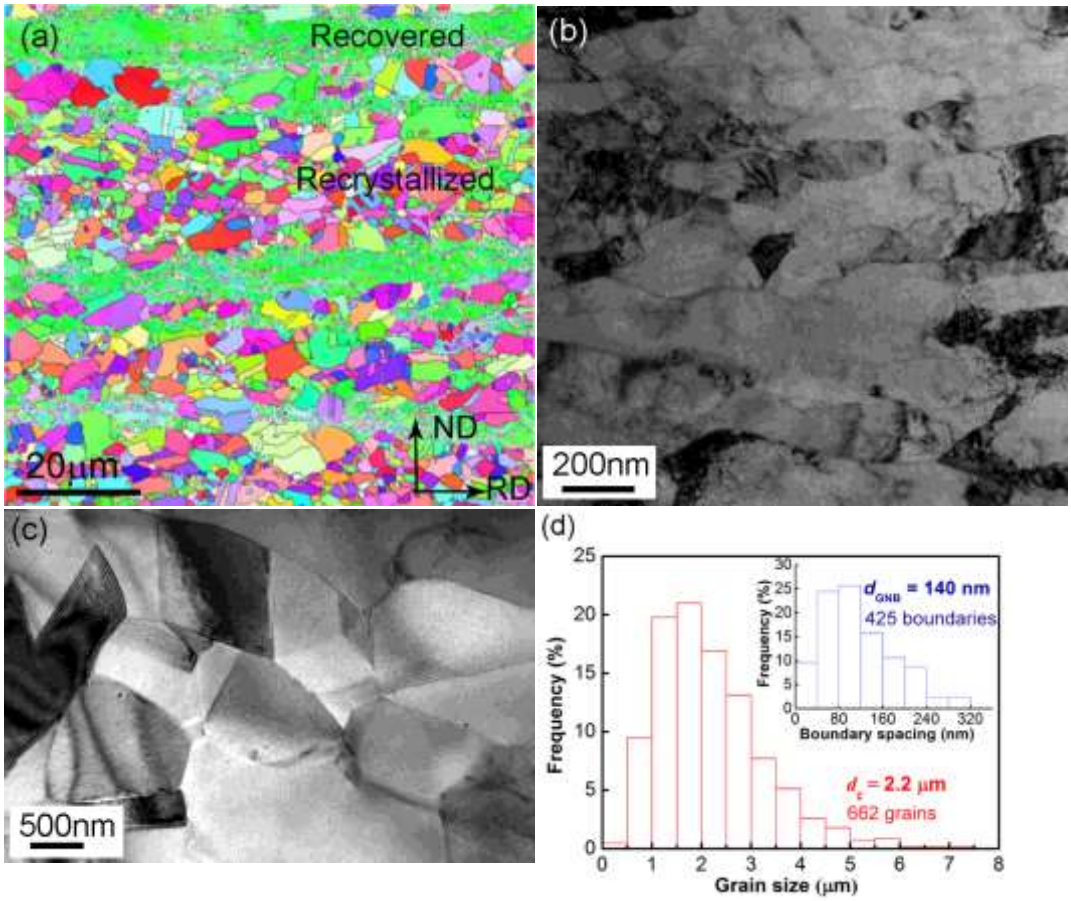

Fig. 3. (a) EBSD orientation map showing the laminated composite structure, (b) TEM image of a recovered lamellar structure delineated by GNBs, (c) TEM image of a recrystallized fine grain structure, and (d) the distribution of GNB spacings and grain sizes in the sample cold rolled to 90% and annealed for 1 hour at 600 °C.

3. Results

3.1 Microstructure

In the cold rolled state the microstructure is characterized by a lamellar structure with the lamellar boundaries approximately parallel to the RD (Fig. 2a and Fig. 2b). The lamellar boundaries are categorized into two types: GNBs of low, medium and high angles (Fig. 2a) and deformation induced twin boundaries (TBs) (Fig. 2b). Using TEM images, the volume fraction of the lamellar structure delineated by the GNBs and that of deformation twins were measured to be 81.2% and 18.8%, respectively. The boundary spacings were measured separately for the GNBs and TBs along the direction perpendicular to the boundaries, and the distributions of measured values are shown in

Fig. 2c. The average values were 53 nm and 21 nm for the GNBs and TBs, respectively.

After annealing for 1 hour at 600°C, the deformed lamellar structure changes into a composite structure of alternating narrow recovered layers and wide recrystallized layers. An example of EBSD orientation maps showing such a composite structure is illustrated in Fig. 3a. The volume fractions of recovered and recrystallized layers were measured to be 10% and 90%, respectively. TEM observations of the recovered structure and the recrystallized structure are shown in Fig. 3b and Fig. 3c. It is seen in Fig. 3b that the recovered layer consists of coarsened lamellar boundaries (Fig. 3b). The spacings between lamellar boundaries were measured from TEM images and their distribution is plotted in Fig. 3d showing an average value of 140 nm. The recrystallized layers are composed of equiaxed grains with an average size of 2.2 μm (Fig. 3d) which were measured from SEM images. Annealing for 1 hour at 1000°C led to a complete recrystallization forming a relatively coarse grain structure that contains many annealing twins (Fig. 4a). By taking the twin boundaries into account, the average grain size was measured to be 21.0 μm, see Fig. 4b.

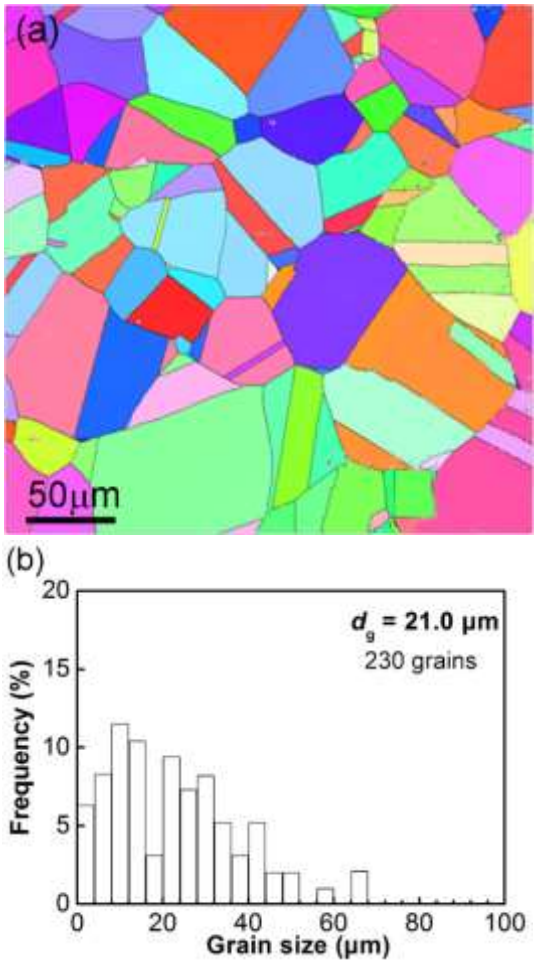

Fig. 4. (a) EBSD orientation map showing the recrystallized grain structure containing annealing twins and (b) the distribution of grain sizes in the sample cold rolled to 90% and annealed for 1 hour at 1000 °C.

The structural features for the above three samples are summarized in Table 1.

Table 1 Structural features and tensile properties of Fe-34.5Mn-0.04C steel samples after different treatments and tested at room temperature

Sample	Treatment	Structural feature	Yield strength (MPa)	UTS (MPa)	Uniform elongation (%)	Total elongation (%)
1	90% Cold rolling (90% CR)	Lamellar structure delineated by GNBs and TBs	1058±10	1242±9	2.0±0.2	7.3±0.2
2	90% CR + 600 °C, 1h	Laminated composite	455±6	644±7	33.0±0.5	39.4±0.1

		structure (Partially recrystallized)				
3	90% CR + 1000 °C, 1h	Recrystallized equiaxed grain structure	211±3	499±6	31.8±0.5	32.7±0.5
4	90% CR + 600 °C, 1h + 5 % CR	Laminated composite structure + dislocations	600±6	677±6	21.8±0.5	35.7±0.7

3.2 Tensile behavior

Fig. 5 shows the engineering stress-strain curves for the cold rolled, partially recrystallized and fully recrystallized samples. The tensile properties are summarized in Table 1. The cold rolled sample with a lamellar structure (curve 1 in Fig. 5a) shows a continuous flow and a high yield stress (0.2% offset) of 1058 MPa. However, the tensile instability sets in at a strain of only 2%, showing a behavior typical of high strain metals. The partially recrystallied sample with a laminated composite structure (curve 2 in Fig.5a) shows a discontinuous flow associated with a yield flateau stress of 455 MPa and 2.2% Lüders elongation, followed by an extensive work hardening stage that leads to a total elongation of 39.5%. The fully recrystallized sample with a coarse grain structure (curve 3 in Fig. 5a) shows also a continuous flow. The yield strength and total elongation were measured to be 211 MPa and 32.7%, respectively. Note that not only the strength but also the tensile ductility of the fully reccrystallized coarse grain sample are lower than the values observed in the laminated composite sample (compare curves 2 and 3 in Fig. 5a, and see Table 1).

The work-hardening rates of the above three samples were calculated from their corresponding true stress-true strain curves and are shown in Fig. 5b. All three samples exhibit the occurrence of tensile instability following the Considère's Criterion:

$$\frac{d\sigma}{d\varepsilon} = \sigma$$

where σ and ε are the true stress and true strain, respectively. However, the evolution of work hardening rate shows significant differences between them. The work

hardening rate of the cold rolled sample drops (curve 1) rapidly, intersecting the true stress-strain curve soon after yielding. For the laminated composite sample (curve 2), the work hardening rate shows a drop during the Lüders deformation and then a rapid increase up to a true strain of 0.05, followed by a gradual decrease during further straining. Note that over the true strain range from 0.05 to failure, the work hardening rate curve of the fine structured laminated composite sample is above that of the fully recrystallized coarse grain sample (compare curves 2 and 3 in Fig. 5b) although their difference is not large. The enhanced work hardening ability is responsible for the improved ductility observed in the laminated composite, which will be discussed in the next section.

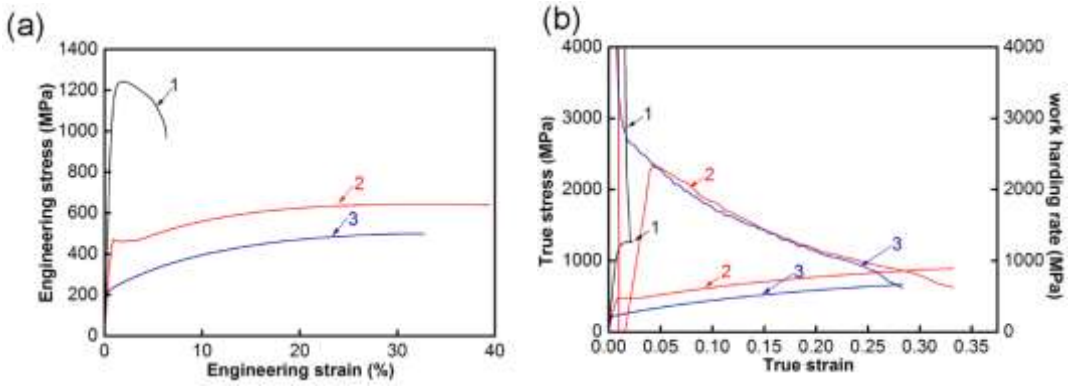

Fig. 5. (a) Engineering stress-strain curves of three different samples (sample 1-3, see Table 1) and (b) their corresponding work hardening rates.

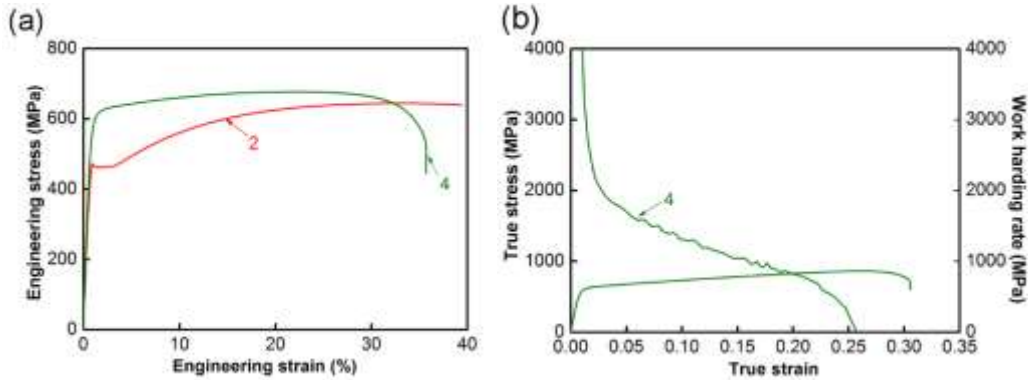

Fig. 6. (a) Engineering stress-strain curves of the laminated composite structure (sample 2) and the laminated composite structure plus 5% additional cold rolling (sample 4), and (b) the work hardening rate for sample 4.

4. Discussion

The laminated composite structure contains hard and soft layers/lamellae which in the present study is obtained by applying a simple processing route of cold rolling and annealing. The formation of such a composite has its cause in the development of a strong rolling texture in the cold rolled sample where texture components are separated by medium and high angle boundaries forming the lamellar structure [15, 23]. The individual lamellae have a characteristic structure and content of stored energy [16]. Therefore, they coarsen at different rates during annealing, which makes it possible to choose annealing conditions at which the structure that combines soft and hard lamellae can form. This structure therefore is a typical laminated composite structure. Note that in the present laminated composite sample, the hard recovered layers only have a volume fraction of 10% and the layer thickness varies from layer to layer. Therefore, the laminated composite structure is not uniform and the volume fractions of the soft and hard layers are not optimized. However, what important is the observation that the presence of only 10% hard recovered lamellae has generated work hardening rates higher than that of the fully recrystallized coarse grain sample. Further improvement in the design of the structural parameters and in the combination of strength and ductility are expected, which is an ongoing study

The microstructure in all three sample states, cold deformed, partially recrystallized and fully recrystallized (Table 1), have that in common, i.e. they are subdivided by medium to high angle boundaries which act as barriers to dislocation glide. The barrier strength can be analyzed based on a Hall-Petch formulation expressing that the yield stress and flow stress is inversely proportional to the square root of the distance between the boundaries. In the deformed and recovered structures, the boundary spacing is determined as the perpendicular spacing between the GNBs and TBs, measured perpendicular to the rolling plane. For the recrystallized structure the boundary spacing is the diameter of the equivalent grain size. The difference in flow stress (0.2% offset) is very large between the recovered and recrystallized layers in the laminated composite due to a large difference in boundary spacing and a deformed nature in the hard layer. The difference in flow stress between layers will for a given external load lead to heterogeneous plastic deformation in the sample. This may give

rise to strengthening mechanisms increasing the strength above the strength that can be analyzed by the rule of mixture typically applied for a composite structure. This difference can be calculated to be the order of 150 MPa indicating a contribution of a hardening mechanism which may have its cause in the heterogeneous plastic deformation giving rise to hardening of the soft layer by the formation of geometrically necessary dislocations [24]. Similar effect has been observed in a heterogeneous lamella structure in Ti and discussed in detail by Wu et al [10].

Besides the constraint effect in the recovered sample, a yield drop phenomenon and Lüders elongation is observed which may also affect the mechanical behavior. This has been observed in a number of experiments (Al [25-2], IF steel [25,28], austenitic steel [29], Ti [10,30]) where the phenomena may have their cause in the lack of mobile dislocations and an increase in stress is required to activate dislocations [31].

The observation of hardening related to the occurrence of a constraint effect introducing extra dislocations together with the yield point phenomenon has led to the experiment where a laminated composite sample is further slightly deformed by cold rolling, as did for a fine structured Al [31]. This additional cold rolling (5%) introduced tangle dislocations in the structure, which was revealed by TEM observations (not shown here), and led to a significant increase in flow stress of about 150 MPa (curve 4 in Fig. 6a) with maintaining reasonably high work hardening rate (Fig. 6b). As a result we have obtained about a 3 times increase in flow stress compared to the recrystallized state with only 10% reduction in uniform elongation (compare Fig. 6 and Fig. 5 and see Table 1).

5. Conclusion

A laminated composite structure in Fe-34.5Mn-0.04C has been processed by cold rolling and annealing. Tensile tests at room temperature were carried out in three sample conditions: cold rolled, partially recrystallized and fully recrystallized. The conclusions are the following:

1. It has been demonstrated that a heterogeneous lamella structure can be produced by

cold rolling and annealing of a single phase alloy forming a laminated composite of hard (recovered) lamellae and soft (recrystallized) lamellae.

2. In the partially recrystallized sample, the mechanical behavior shows a doubling of the yield strength compared to recrystallized sample without a loss of ductility. Additional deformation by cold rolling results in a further 50% increase in strength with only 10% loss in uniform elongation, which also removes the yield drop phenomenon.
3. The excellent mechanical properties of the partially recrystallized state are interpreted based on the rule of mixture with additional strengthening contributions related to the heterogeneous plastic deformation and the occurrence of a yield drop phenomenon.

Acknowledgements

The authors gratefully acknowledge the support from the National Natural Foundation of Hebei Province, China (Grant No. E2018203312). XH thanks the support of State Key Research and Development Program of MOST of China (2016YFB0700401). NH thanks the support of the 111 Project (B16007) by the Ministry of Education and the State Administration of Foreign Experts Affairs of China.

References

[1] Y. T. Zhu, X. Z. Liao, Nature Mater. 3 (2004) 351-352.

[2] R. Z. Valiev, I. V. Alexandrov, Y. T. Zhu, T. C. Lowe, J. Mater. Res. 17 (2002) 5–8.

[3] M. A. Meyers, A. Mishra, D. J. Benson, Prog. Mater. Sci. 51(2006) 427-556.

[4] L. Lu, Y. F. Shen, X. H. Chen, L. H. Qian, K. Lu, Science 304 (2004) 422–426.

[5] X. L. Wu, P. Jiang, L. Chen, F. P. Yuan, Y. T. Zhu, Proc Natl Acad Sci U.S.A. 111 (2014) 7197–7201.

[6] B. Hu, H. W. Luo, F. Yang, H. Dong, J. Mater. Sci. Technol. 33 (2017) 1457-1464.

[7] X. X. Huang, Hansen N, and Tsuji N, Science 312 (2006) 249-251.

[8] T. H. Fang, W. L. Li, N. R. Tao, K. Lu, Science 331 (2011)1587 -1590.

[9] Y. M. Wang, M.W. Chen, F. H. Zhou, E. Ma, Nature 419 (2002) 912-915.

[10] X. L. Wu, M. X. Yang, F. P. Yuan, G. L. Wu, Y. Wei, X. X. Huang, Y. T. Zhu, Proc. Natl. Acad. Sci. U.S.A. 112 (2015) 14501-14505.

[11] D. Kuhimann-Wilsdorf, N. Hansen, Scripta Metall. Mater. 1991 (25) 1557-1562.

[12] N. Hansen, Mater. Trans. A 32A (2001) 2001-2917.

[13] J. A. Wert, Proc. 19th Risø Int. Symp. On Materials Science, J. V. Carstensen, T. Leffers, T. Lorentzen, O. B. Pedersen, B. F. Sørensen, and G. Winther, eds. Risø National Laboratory, Roskilde, 1998, 573-584.

[14] D. A. Hughes, N. Hansen, Acta Mater. 48 (2000) 2985-3004.

[15] G. L. Wu, D. Juul Jensen, Mater. Sci. Tech. 21 (2005)1407-1411.

[16] Q. Xing, X. X. Huang, N. Hansen, Mater. Trans. A 37A (2006) 1311-1322.

[17] X. X. Huang, Q. Xing. D. Juul Jensen, N. Hansen, Mater. Sci. Forum 519-521 (2006) 79-84.

[18] Y. Tomota, M. Strum, J.W. Morris Jr., Metall. Trans. A . 17A (1987) 1073-1081.

[19] O. Grässel, L. Kruger, G. Frommeyer, L.W. Meyer, Int. J. Plast. 16 (2000) 1391-1409.

[20] L.Q. Chen, Y. Zhao, X.M. Qin, Acta Metall. Sin (Engl. Lett.), 26 (2013) 1-15.

[21] S. S. Sohn, S. Hong, J. Lee. B-C. Suh, S-K. Kim, B-J Lee, N.J. Kim, S. Lee, Acta Mater. 100 (2015)39-52.

[22] X. Y. Yuan, Y. Zhao, X. Li, L.Q. Chen, J. Mater. Sci. Technol. 33 (2017) 1555-1560.

[23] Q. Liu, X. X. Huang, D. J. Lloyd, N. Hansen, Acta Mater. 50 (2002) 3789-3802.

[24] M. F. Ashby, Philos. Mag. 21 (1970) 399-411.

[25] N. Tsuji, Y. Ito, Y. Saito, Y. Minamino, Scripta Mater,47 (2002) 893-899.

[26] C. Y. Yu, P. W. Kao, C. P. Chang, Acta Mater. 53 (2005) 4019-4028.

[27] N. Kamikawa, X. Huang, N. Tsuji, N. Hansen, Acta Mater. 570 (2009) 4198-4208.

[28] S. Gao, M. C. Chen, M. Joshi, A. Shibata, N. Tsuji. J. Mater. Sci. 49(19) (2014) 6536-6542.

[29] R. Ueji, N. Tsuchida, D. Terada, N. Tsuji, Y. Tanaka, A. Takemura, K. Kunishige, Scripta Mater 59 (2008) 963-66

[30] Z. Li, L. Fu, B. Fu, A. D. Shan, Mater Lett. 96 (2013) 1-4.

[31] X. Huang. Scripta Mater. 60 (2009) 1078-1082.